BEILSTEIN JOURNAL OF NANOTECHNOLOGY

Ultrasonication-assisted synthesis of $CsPbBr_3$ and Cs_4PbBr_6 perovskite nanocrystals and their reversible transformation

Longshi Rao[1,2], Xinrui Ding*[1], Xuewei Du[1], Guanwei Liang[1], Yong Tang[1], Kairui Tang[3] and Jin Z. Zhang[2]

Full Research Paper

Open Access

Address:
[1]Engineering Research Centre of Green Manufacturing for Energy-Saving and New-Energy Technology, School of Mechanical and Automotive Engineering, South China University of Technology, Guangzhou 510640, China, [2]Department of Chemistry and Biochemistry, University of California, Santa Cruz, CA 95064, USA and [3]Mechanical Engineering, Pennsylvania State University, Harrisburg, PA 17057, USA

Email:
Xinrui Ding* - dingxr@scut.edu.cn

* Corresponding author

Keywords:
$CsPbBr_3$ PNCs; Cs_4PbBr_6 PNCs; polar-solvent-free; reversible transformation; ultrasonication

Beilstein J. Nanotechnol. **2019,** *10,* 666–676.
doi:10.3762/bjnano.10.66

Received: 31 October 2018
Accepted: 13 February 2019
Published: 06 March 2019

This article is part of the thematic issue "Low-dimensional materials and systems".

Guest Editor: S. Walia

Abstract

We demonstrate an ultrasonication-assisted synthesis without polar solvent of $CsPbBr_3$ and Cs_4PbBr_6 perovskite nanocrystals (PNCs) and their reversible transformation. The as-prepared $CsPbBr_3$ PNCs and Cs_4PbBr_6 PNCs exhibit different optical properties that depend on their morphology, size, and structure. The photoluminescence (PL) emission and quantum yield (QY) of the $CsPbBr_3$ PNCs can be tuned by changing the ultrasound power, radiation time, and the height of the vibrating spear. The optimized $CsPbBr_3$ PNCs show a good stability and high PL QY of up to 85%. In addition, the phase transformation between $CsPbBr_3$ PNCs and Cs_4PbBr_6 PNCs can be obtained through varying the amount of oleylamine (OAm) and water. The mechanism of this transformation between the $CsPbBr_3$ PNCs and Cs_4PbBr_6 PNCs and their morphology change are studied, involving ions equilibrium, anisotropic growth kinetics, and CsBr-stripping process.

Introduction

Metal halide perovskite nanocrystals (PNCs) are promising candidates for application in the fields of light-emitting diodes (LEDs) [1,2], high-efficiency solar cells [3], low-threshold lasers [4], and photodetectors [5]. Compared to traditional semiconductors, colloidal PNCs demonstrate excellent properites, such as tunable photoluminescence (PL) throughout the visible spectrum, super high PL quantum yield (QY), low trap-state density, and narrow emission linewidth [6-8]. The crystal structure of $CsPbX_3$ ($X = Cl^-$, Br^-, I^-) PNCs consists of a 12-fold coordinated network created by $[PbX_6]^{4-}$ octahedra in which the Cs^+ ions reside in the periphery of this network [9,10]. These PNCs are prone to structural instabilities and phase trans-

formations involving ion migration and interface hydration [11]. However, this phase and structure versatility has become the great advantage of PNCs in their technical applications, especially in optoelectronics. Although the focus has been on the $CsPbX_3$ structure, researchers start to turn their attention on synthesizing new perovskite materials, such as Cs_4PbX_6 PNCs. Under Cs-rich or Pb-poor synthesis conditions, zero-dimensional (0D) structures of Cs_4PbX_6 NCs can be achieved, demonstrating a crystalline structure with well-separated octahedra $[PbBr_6]^{4-}$ isolated by Cs^+ ions [12,13]. This specific structure is expected to result in strong quantum confinement and electron–phonon interactions. This inspires researchers to further explore this structure. The key to this exploration is the development of various approaches to the synthesis of high-quality PNCs.

Since, in 2015, Kovalenko and co-workers synthesized $CsPbX_3$ PNCs by using a hot-injection method, great successes in the controlled synthesis and application of the $CsPbX_3$ PNCs have been achieved in a very short time [14]. To date, the most commonly adopted approach for synthesizing highly efficient PNCs are solution-based procedures, including hot injection, solvothermal synthesis, microreactor synthesis, and room-temperature (RT) ligand-mediated reprecipitation, in which shape and size are tuned through the control of temperature, reaction time, and composition of the precursors [15-17]. Chen et al. demonstrated a facile solvothermal method for preparing $CsPbX_3$ PNCs with adjustable optical properties [18]. Additionally, Li's group reported a poly(lactic acid)-assisted anion-exchange method using a microreactor for tuning the emission spectra of $CsPbX_3$ PNCs from green to near-ultraviolet, which might be applicable for mass production [19]. Besides, great efforts have been made to prepare PNCs through the chemical transformation of pre-synthesized PNCs [20-22]. For example, Wu et al. reported a CsX-stripping method that enabled the transformation of nonluminescent Cs_4PbX_6 PNCs to highly luminescent $CsPbX_3$ PNCs through an interfacial reaction [20]. They focus on investigating the water-triggered transformation process between Cs_4PbX_6 PNCs and $CsPbX_3$ PNCs in a different phase. Similar methods were applied to explore new perovskite materials such as Cs_4PbBr_6. Zhai et al. showed a simple solvothermal approach for synthesizing $CsPbBr_3$ nanoplatelets and their phase transformation to Cs_4PbBr_6 PNCs [23]. Liu and co-workers also demonstrated that $CsPbBr_3$ PNCs were successfully converted to Cs_4PbBr_6 PNCs through a "ligand-mediated transformation" method with the addition of oleylamine (OAm) [24]. Udayabhaskararao's group showed the reversible transformation from $CsPbX_3$ to Cs_4PbX_6 through the ratio of oleic acid (OA) to OAm in a Brønsted acid–base equilibrium [25]. Despite the progress made in obtaining PNCs, in general, inert conditions, high temperature and pre-synthesized precursors are required for hot injection. In addition, RT methods were mostly carried out by mixing a polar solvent with a large amount of nonpolar solvent. Since PNCs are reported to be very sensitive to polar solvents, these methods result in the inevitable degradation of PNCs, especially for iodine-based PNCs [26-28]. Therefore, in order to obtain PNCs with high PL QY and stability, it is crucial to develop synthesis methods free of polar-solvents.

To date, some attempts have been made to synthesize PNCs without the use of polar solvents. Tong's group demonstrated the single-step and polar-solvent-free synthesis of $CsPbX_3$ PNCs with tunable halide ion composition and thickness through the direct ultrasonication of precursors [29]. Whereas this method has been reported for synthesizing PNCs without using polar solvents, it does not allow for a control over dimensionality and phase transformation. We recently reported a fast, low-cost, environmentally friendly, and polar-solvent-free strategy for synthesizing all-inorganic $CsPbBr_3$ NCs with tunable shape and size [30]. During this process, we found that a great excess of OAm results in the formation of a derivative of $CsPbBr_3$ NCs, i.e., Cs_4PbBr_6. However, the underlying transformation mechanism has not been fully understood. Following this, we set out here to expand this study to control the phase transformation. $CsPbBr_3$ PNCs as precursor were obtained by modifying the approach initially presented by Tong, which was recently elaborated by our group [29,30]. We demonstrated in detail how, by tuning the ultrasound power and time, the PL emission of $CsPbBr_3$ PNCs can be precisely controlled. Benefitting from this knowledge, here we attained $CsPbBr_3$ PNCs with a high PL QY (ca. 85%) by optimizing the immersion height of the vibrating spear in the liquid. In addition, the phase transformation of $CsPbBr_3$ PNCs to Cs_4PbBr_6 PNCs was achieved in this study by direct ultrasonication of solid powders or by adding OAm in the solution of pre-synthesized $CsPbBr_3$ PNCs. Finally, inspired by the method proposed by Wu et al. [20], a successful structure conversion from Cs_4PbBr_6 PNCs to $CsPbBr_3$ PNCs was obtained here by simply adding different amounts of water into pre-synthesized Cs_4PbBr_6 PNCs. The mechanism behind phase transformation and morphology change were investigated by using a combination of spectroscopy and microscopy techniques.

Results and Discussion

Characterization of $CsPbBr_3$ PNCs

The typical procedure for synthesizing $CsPbBr_3$ and Cs_4PbBr_6 PNCs and for reversibly transforming them is illustrated in Scheme 1. Cs_2CO_3 and $PbBr_2$ were loaded into the liquid paraffin/OAm/OA solution. Then, the precursors were processed by tip-sonication and purified via centrifuging in the presence of methyl acetate as precipitation agent. Subsequently,

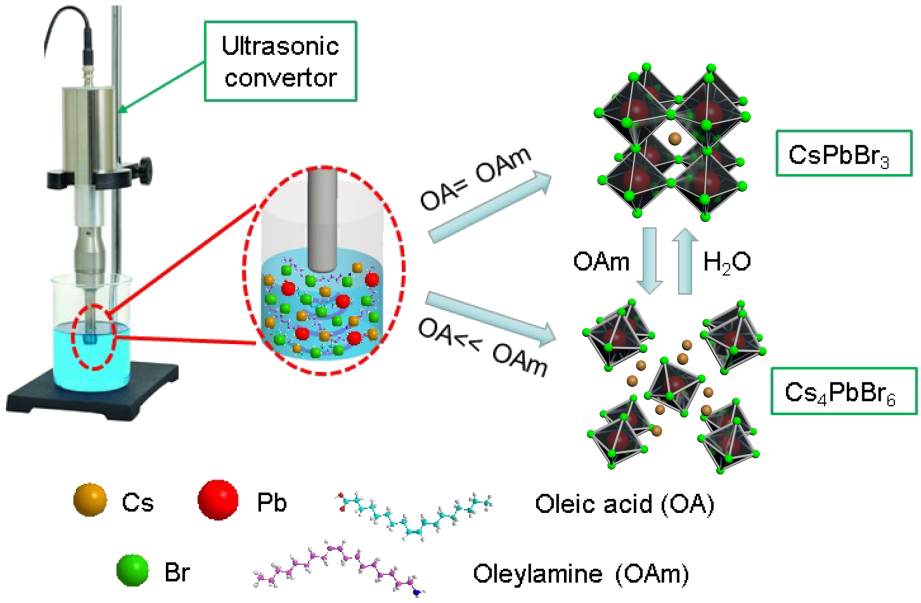

Scheme 1: Illustration of synthesizing $CsPbBr_3$ and Cs_4PbBr_6 PNCs without polar solvent using ultrasonication assistance, and their reversible transformation by adding OAm and water.

the sediment was redispersed in toluene for further characterization. The reversible transformation between Cs_4PbBr_6 PNCs and $CsPbBr_3$ PNCs was achieved by changing the amounts of OAm and water. Detailed synthesis conditions are given in the Experimental section.

The crystal structure and morphology of the as-prepared samples were determined by XRD and TEM. As shown in Figure 1a, the diffraction pattern clearly indicates that orthorhombic $CsPbBr_3$ PNCs (PDF card #18-0364) were formed. No other phases were observed, suggesting the high

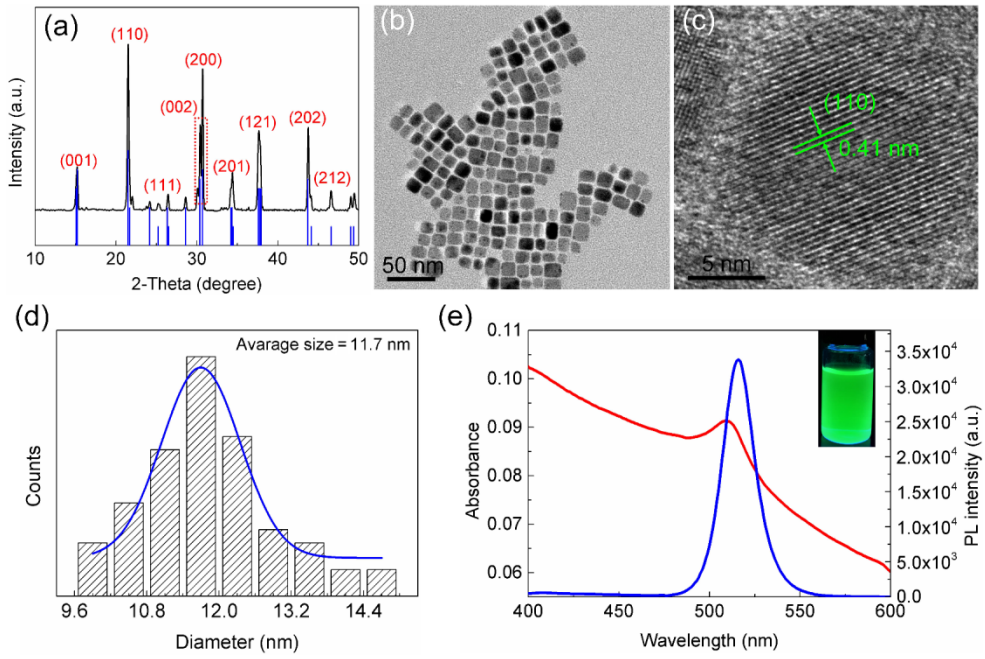

Figure 1: Characterization of the $CsPbBr_3$ PNCs prepared using ultrasonication assistance. (a) XRD patterns. Black line and blue line represent experimental data and standard reference, respectively. (b) TEM image. (c) HRTEM image. (d) Size distribution. (e) UV–vis absorption spectrum (red line) and PL emission spectrum (blue line). Inset is a photograph under 365 nm UV irradiation.

purity of the samples. The TEM image shown in Figure 1b demonstrates that the $CsPbBr_3$ PNCs have a regular square morphology. HRTEM was further carried out to measure the lattice spacing of the product. Figure 1c shows a lattice spacing distance of ca. 0.41 nm for the $CsPbBr_3$ PNCs. The size distribution shown in Figure 1d indicates that the well-dispersed $CsPbBr_3$ PNCs have an average diameter of ca. 11.7 nm. To explore the optical properties of colloidal $CsPbBr_3$ PNCs, UV–vis absorption spectra and PL emission spectra were recorded. As shown in Figure 1e, the first excitonic absorption peak was located at 510 nm and the strong PL emission band centered at 516 nm was observed with a narrow full width at half maximum (FWHM) of 18 nm, indicating a narrow polydispersity of the PNCs obtained by this method. The PL QY of the as-prepared $CsPbBr_3$ PNCs measured to be ca. 85% (Rhodamin 101 as reference, PL QY is 100%) following a previously published report [31]. In addition, Supporting Information File 1, Figure S1 clearly demonstrates the improved photostability and chemical stability of $CsPbBr_3$ PNCs.

Effect of synthesis conditions

Our previous study has shown that ultrasound power and radiation time have a great influence on the optical properties of the $CsPbBr_3$ PNCs [30]. In this study, we found that the immersion height of the vibrating spear in the solvent influences the product properties (the effect will be discussed later). We divided the height of liquid into five equal parts, i.e., from the bottom to the surface of the liquid, 1/5, 2/5, 3/5, 4/5, and 5/5.

We first investigated the effect of ultrasound power on the optical properties of $CsPbBr_3$ PNCs. To avoid breaking the bottle, the immersion height of the vibrating spear and radiation time are 4/5 and 30 min, respectively. Figure 2a shows the change of UV–vis absorption spectra and PL spectra of the $CsPbBr_3$ PNCs that were synthesized at 90, 120, 150, 180, and 210 W of ultrasound power, while keeping other synthesis conditions unchanged. If the ultrasound power is less than 90 W, there is no UV–vis absorption peak and a very weak PL intensity, implying that almost no PNCs formed. However, the first characteristic absorption peak changes to red slowly with an increase of ultrasound power, corresponding to the red-shift of the PL emission peak, which is similar to the findings we recently reported [30]. While higher ultrasound power supports faster dissolution, it has also a strong impact on the homogeneity of the PNCs. For example, when the ultrasound power is 210 W, the UV–vis absorption at long wavelengths is very high, indicating large crystals were formed with strong scattering. Therefore, it is necessary to choose the appropriate ultra-

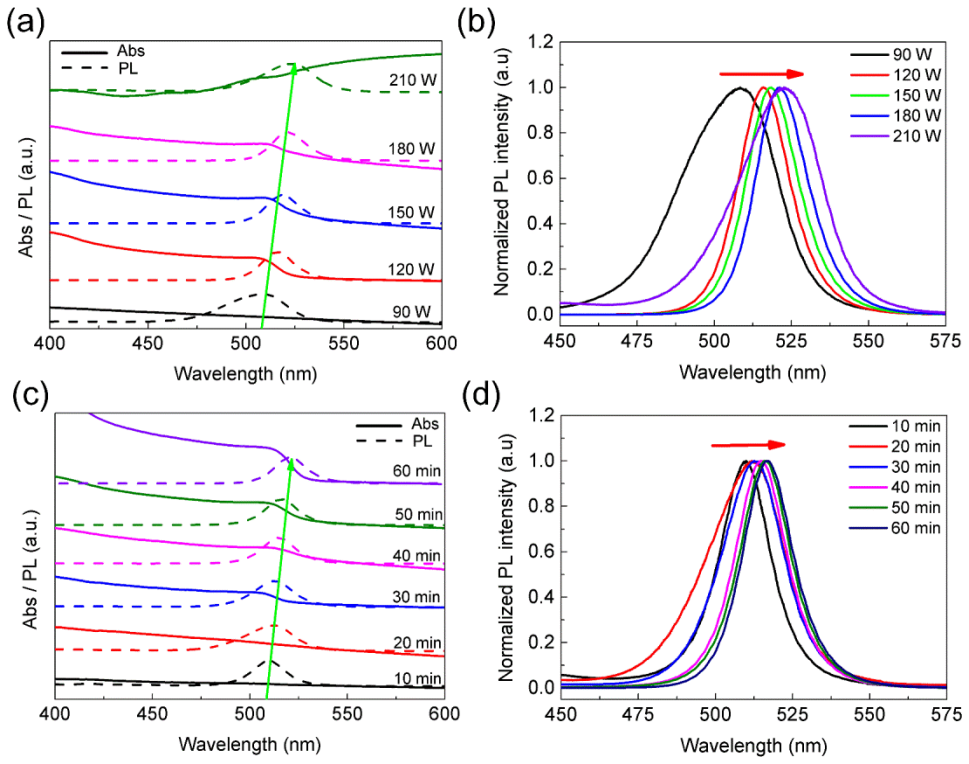

Figure 2: (a) UV–vis absorption spectra and PL emission spectra, and (b) normalized PL emission spectra of the $CsPbBr_3$ PNCs that were synthesized at 90, 120, 150, 180, and 210 W of ultrasound power, respectively. (c) UV–vis absorption spectra and PL spectra, and (d) normalized PL emission spectra of $CsPbBr_3$ PNCs that were synthesized at 10, 20, 30, 40, 50, and 60 min of radiation time.

sound power. The normalized PL emission peaks in Figure 2b shift from 505 to 523 nm, indicating that our approach can precisely modulate PL emission.

Furthermore, we studied the influence of radiation time on the $CsPbBr_3$ PNCs. The immersion height of the vibrating spear and ultrasound power are 4/5 and 120 W, respectively. As shown in Figure 2c and Figure 2d, when the radiation time is increased, both the UV–vis absorption and PL spectra are redshifted, we suggest that it is the size effect that is dominant over ionic bond strength in causing the spectral shift, which is different from the effects of radiation time that we observed recently [30]. This phenomenon indicates that the immersion height of the vibrating spear would affect PNCs properties.

The effects of the immersion height of the vibrating spear in the liquid were also investigated. The total liquid height was divided into five equal parts as shown in the inset of Figure 3a. Figure 3a shows the PL intensity (UV–vis absorbance at 400 nm) of four samples that were synthesized by setting the immersion height of the vibrating spear to 1/5, 2/5, 3/5, and 4/5 of the total liquid height. As the immersion height increases, the corresponding PL intensity obviously decreases. In addition, the PL QY in Figure 3b further confirmed that the $CsPbBr_3$ PNCs exhibit the best performance when the immersion height of the vibrating spear is set at 1/5 of the total liquid height. Ultrasonication results in a combination of thermal, vibrational, and acoustic cavitation, i.e., the formation, growth, and implosive collapse of bubbles in liquids [32-34]. In the center of these bubbles, extremely high temperatures of about 5000 K and high pressures of about 20 MPa were achieved by high-intensity ultrasound [32], enabling a quick decomposition of the particles. The lower the immersion height of vibrating spear, the higher temperature and pressure is achieved, which, as a result, benefits the formation of PNCs.

Characterization of Cs_4PbBr_6 PNCs

The current approach can be further used for controlling phase and structure transformations in the PNCs. The method introduced in this work enables the successful synthesis of rhombohedral Cs_4PbBr_6 PNCs via changing the amount of OAm. The amount of OAm was increased to 3.0 mL, while all other conditions were kept the same. The phase of the obtained product was characterized by XRD, as shown in Figure 4a. The XRD pattern with peaks at 2θ = 12.9, 20.1, 22.4, 25.6, 28.6 30.3, 30.9, 34.1, 39.3, and 45.7° correspond to diffractions from (110), (113), (300), (024), (214), (223), (006), (134), (330), and (600) crystal planes of rhombohedral Cs_4PbBr_6 (PDF card #73-2478) [13]. Meanwhile, weak peaks of $CsPbBr_3$ were observed, indicating both $CsPbBr_3$ and Cs_4PbBr_6 PNCs were formed during the process.

TEM was further performed to characterize the morphology of as-prepared PNCs. Figure 4b shows the formation of Cs_4PbBr_6 PNCs with hexagonal crystal structure and confirms the existence of square-shaped $CsPbBr_3$ PNCs. Additionally, Figure 4c shows that the small black spots (green arrows) existing on the surface of the Cs_4PbBr_6 PNCs are metallic lead nanoparticles that have been reported before [23,35,36]. The HRTEM image shown in Figure 4d demonstrates an interplanar spacing of 0.39 nm, corresponding to the (300) crystal plane of bulk Cs_4PbBr_6, which is also consistent with the PDF card #73-2478. The size of the Cs_4PbBr_6 PNCs is defined here as the longest distance between hexagonal corners, which is ca. 65 nm for the example shown. Besides, the SEM image illustrates that Cs_4PbBr_6 particles are hexagonal prisms with a thickness of ca. 15 nm, as presented in Figure 4d inset and Supporting Information File 1, Figure S2.

The absorption spectrum of the Cs_4PbBr_6 PNCs is very different from that of the $CsPbBr_3$ PNCs, as shown in Figure 4e. The

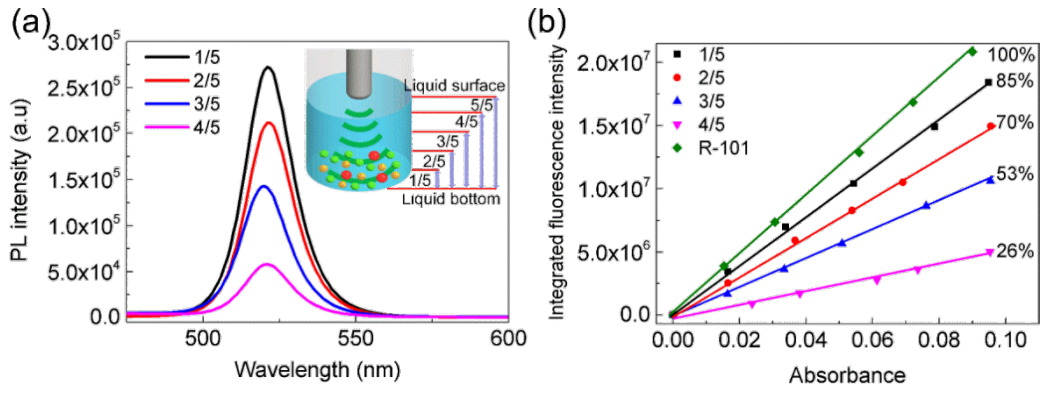

Figure 3: (a) PL emission spectra and (b) PL QY of the $CsPbBr_3$ PNCs that were synthesized at 1/5, 2/5, 3/5, and 4/5 of total liquid height, respectively. 1/5, 2/5, 3/5, 4/5, and 5/5 in (a) inset is one of the five equal parts from liquid bottom to liquid surface. R-101 in (b) is rhodamine 101 (PL QY, 100%) as the standard sample to test PL QY of PNCs.

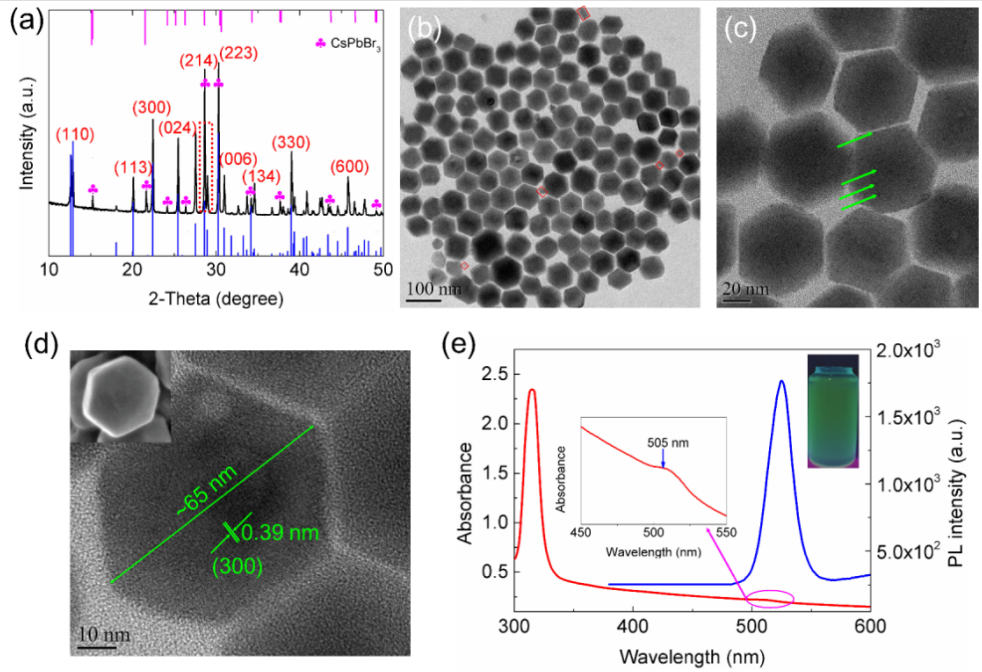

Figure 4: Characterization of the Cs_4PbBr_6 PNCs synthesized using ultrasonication. (a) XRD patterns. Black line represents experimental data; blue line (below) and pink line (upper) represent standard reference bulk $CsPbBr_3$ and Cs_4PbBr_6, respectively. (b) TEM image, red squares represent $CsPbBr_3$ PNCs. (c),(d) HRTEM images, green arrows in (c) represent metallic lead nanoparticles and inset in (d) is SEM image of Cs_4PbBr_6 PNCs, respectively. (e) UV–vis absorption spectra (red line) and PL emission spectra (blue line). Insets are high resolution absorption spectrum and representative digital photograph.

first excitonic absorption has been shifted from 510 nm for $CsPbBr_3$ PNCs to 315 nm for Cs_4PbBr_6 PNCs. This absorption feature is consistent with that of bulk Cs_4PbBr_6, which was proven to be the localized $6s_{1/2}$–$6p_{1/2}$ transition within the isolated $[PbBr_6]^{4-}$ octahedra separated by Cs^+ ions [24]. A weak characteristic UV–vis absorption and a PL emission peak for $CsPbBr_3$ PNCs at 505 nm and 520 nm, respectively, further confirmed the existence $CsPbBr_3$ PNCs.

In Cs_4PbBr_6 PNCs, typically a green emission arises either from defects or from impurities or from a combination of both [37,38]. Herein, the purified Cs_4PbBr_6 PNCs did not demonstrate PL emission over the whole visible spectrum due to their wide bandgap ($E_g(Cs_4PbBr_6)$ = 3.94 eV), while the observed weak PL emission results from a small portion of $CsPbBr_3$ impurities in the Cs_4PbBr_6 PNCs (see Figure 3a–e). Since $CsPbBr_3$ PNCs exhibit a high PL QY, the green PL emission is ascribed to minor $CsPbBr_3$ impurities in the samples. This result coincides with previous works on Cs_4PbBr_6 PNCs that show a strong green emission at about 500 nm and confirmed that these green PL emissions originate from $CsPbBr_3$ PNC impurities [10,39,40].

Furthermore, the effect of the amount of OAm on the phase transformation was investigated. As shown in Figure 5a, when the amount of OAm ranged from 0.5 to 3.0 mL, the first characteristic absorption peak (ca. 510 nm) and the PL emission intensity of $CsPbBr_3$ PNCs slowly decrease, while new strong absorption features in the UV region (ca. 315 nm) emerge, which have been confirmed to result from the formation of Cs_4PbBr_6 PNCs [25]. When adding equal amounts of OAm and OA, there are no other peaks in the UV–vis absorption spectra except for that at ca. 510 nm. With increasing amount of OAm, the absorption intensity at ca. 510 nm decreases. Simultaneously, the absorption intensity at ca. 315 nm increases, while the PL intensity decreases (Figure 5b), and is blue-shifted followed by an increase in the FWHM of the PL peak. All these effects suggest the decomposition of the $CsPbBr_3$ PNCs. Based on this process it can be concluded that the excess amount of OAm triggers the transformation between $CsPbBr_3$ PNCs and Cs_4PbBr_6 PNCs.

The morphology change from $CsPbBr_3$ PNCs to Cs_4PbBr_6 PNCs was further confirmed by using TEM. When the amount of OAm is between 0.5 and 1.5 mL, the morphology of PNCs gradually becomes irregular and some hexagonal shapes emerge (Figure 5c–e). As the amount of OAm increase to 3.0 mL, Cs_4PbBr_6 PNCs with homogeneous hexagonal shape can be achieved (Figure 5h). These results suggest that the growth kinetics of this process can be controlled by adding OAm, and the PNCs are prone to crystallize in the Cs-rich Cs_4PbBr_6 phase when OAm is present in excess. The transformation from

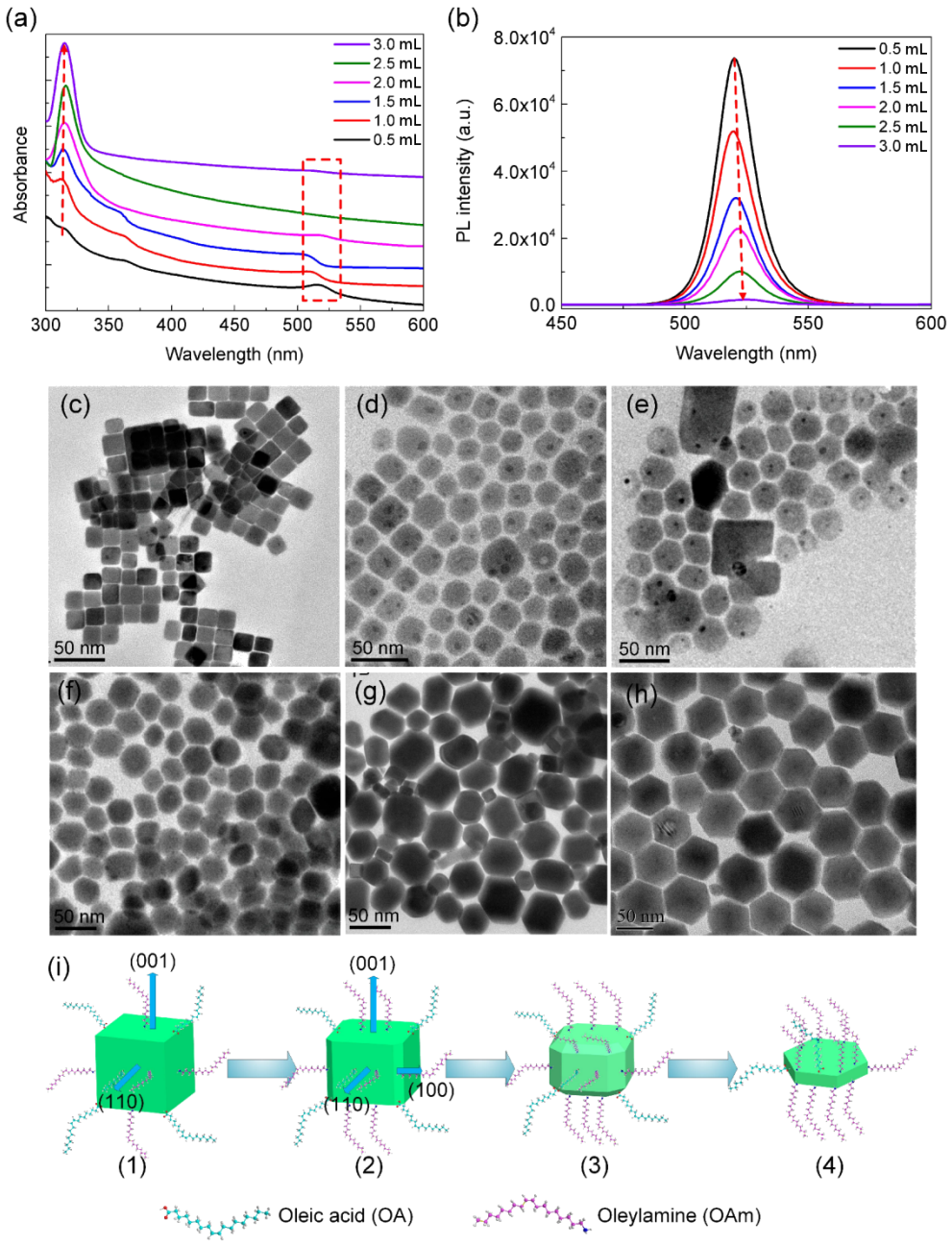

Figure 5: The change of (a) UV–vis absorption spectra, (b) PL spectra, and (c)–(h) TEM images of $CsPbBr_3$ PNCs synthesized at 0.5, 1.0, 1.5, 2.0, 2.5, and 3.0 mL of OAm, respectively, while keeping OA unchanged. (i) Schematic illustration of the morphology change from $CsPbBr_3$ PNCs to Cs_4PbBr_6 PNCs.

$CsPbBr_3$ to Cs_4PbBr_6 leads to a remarkable change in crystal structure and atomic composition. Udayabhaskararao et al. demonstrated that this transformation is driven by recrystallization induced by micelle formation or soft-ligand templating [25]. This mechanism, however, cannot explain the phase transformation from $CsPbBr_3$ to Cs_4PbBr_6 in this work because there are no intermediate stages observed by TEM. Therefore, we suppose the transformation between the two phases involves ion equilibria. A large amount of OAm can form oleylammonium and dissolve $PbBr_2$, resulting in the formation of lead oleate and oleylammonium bromide, thus driving the transformation [41]. An even larger amount of OAm can also dissolve $CsPbBr_3$ PNCs and accelerate the transformation into Cs_4PbBr_6 PNCs. This process is related to Ostwald ripening that was found during the nucleation and growth of PNCs [42]. Therefore, the formation of Cs_4PbBr_6 PNCs is promoted by the capacity of the organic ligands to dissolve $PbBr_2$ and by the dissociation of $CsPbBr_3$ PNCs.

A series of TEM images (Figure 4c–h) clearly confirm that the morphology of these PNCs can be tuned easily by changing the amount of OAm in the precursor solution, while keeping the amount of OA unchanged. We attribute this morphology change to the crystal anisotropy induced by the growth kinetics. The capping ligands are preferentially attached to the PNCs facets, resulting in different growth rates on different crystal facets [43]. A schematic illustration of the morphology change between $CsPbBr_3$ PNCs and Cs_4PbBr_6 PNCs is shown in Figure 5i. When equal amounts of OA and OAm are added, the reaction favors isotropic growth, since OA and OAm play a cooperative role (Figure 5i(1)). When more OAm is added, the long-chain OAm are more easily bound to the surface of the PNCs and restrict the perpendicular growth (001) [44]. Additionally, the growth rates for the side planes are different due to excess amount of OAm easily aggregated at the boundary of two adjacent planes [45], which possibly leads to the formation of (100) planes and the appearance of diamond-like product, as demonstrated in Figure 5i(2,3). This inhibiting effect is distinct when OAm is added in large excess, yielding a hexagonal structure with sharp edges, as shown in Figure 5i(4).

Reversible transformation between Cs_4PbBr_6 PNCs and $CsPbBr_3$ PNCs

After a few weeks, the prepared Cs_4PbBr_6 PNCs solution became milky white, indicating that untransformed $CsPbBr_3$ PNCs decomposed completely. We further explored a possible reversible transformation by introducing different amounts of water. When little water was added, the color of Cs_4PbBr_6 solution changed from colorless to light-green rapidly (Supporting Information File 2), implying a possible structural transformation. In order to monitor the transformation process, different amounts of water were gradually dropped into a Cs_4PbBr_6 PNCs solution (Figure 6a). When more water was added, the solution became green-yellow.

Furthermore, the transformation process was studied by using UV–vis absorption and PL emission spectroscopy. As shown in Figure 6b, the colorless Cs_4PbBr_6 PNCs solution exhibits a strong first excitonic absorption peak at 315 nm. When a small amount of water was slowly added, the intensity of the first excitonic absorption peak declined gradually, indicating the decomposition of Cs_4PbBr_6 PNCs. Correspondingly, a weak absorption peak at 510 nm emerged. Moreover, as the amount of water was increased, the intensity of the absorption peak at about 510 nm increased steadily (inset in Figure 6b). Compared with the excitonic absorption peak of Cs_4PbBr_6 PNCs, the product displayed only weak absorbance. Figure 6c demonstrates the PL emission spectra of the samples during the transformation process. After the addition of small amounts of water, a PL emission peak at 518 nm appeared and gradually increased in intensity, suggesting a luminescent product was formed. XRD measurements were carried out to determine the phase of the obtained product. As shown in Figure 6d, the XRD diffraction pattern of final product is consistent with bulk orthorhombic $CsPbBr_3$ (PDF card #18-0364), suggesting the formation of $CsPbBr_3$ PNCs. Moreover, the PL QY of as-prepared $CsPbBr_3$ PNCs was calculated to be ca. 70%. Interestingly, the $CsPbBr_3$ PNCs show a high stability in ambient environment, as shown in Figure 6e. Upon the addition of a large amount of OAm and upon ultrasonication, the conversion from $CsPbBr_3$ PNCs to Cs_4PbBr_6 PNCs was achieved (Supporting Information File 1, Figure S3) and can be repeated more than two times, similar to previous reports [25].

The addition of led to the decomposition of Cs_4PbBr_6 and the formation of $CsPbBr_3$ PNCs, triggered by the stripping of water-soluble CsBr. During this process, the rhombohedral Cs_4PbBr_6 PNCs are slowly converted to orthorhombic $CsPbBr_3$ PNCs (Figure 6d) and the rate of this conversion depends on the amount of water. The CsBr-stripping can be proven by the reduction of crystal size from 65 to 11.7 nm (Figure 1 and Figure 4). This is consistent with the findings reported by Wu and co-workers [20]. As the solubility of liquid paraffin or capping ligands in water is very low, further dissolution of $CsPbBr_3$ PNCs is inhibited, which is similar to the effect demonstrated by Wu's group who took advantage of the very low (only 9.5 mg/L) solubility of hexane in water [20]. The above result indicates that the $CsPbBr_3$ PNCs have a higher stability than Cs_4PbBr_6 PNCs against water.

Conclusion

In summary, we demonstrate the effect of small changes in the environment of capping ligands and water on the crystal structure and stoichiometry of PNCs. This study expanded our recent work of synthesizing differently shaped $CsPbBr_3$ PNCs [30]. Similarly as demonstrated in our recent study, by changing the ultrasound power and radiation time, the PL emission of $CsPbBr_3$ PNCs could be easily tuned. More importantly, with lower the immersion heights of the vibrating spear higher PL QY of $CsPbBr_3$ PNCs were achieved. The as-prepared $CsPbBr_3$ PNCs show a high PL QY of up to 85% and a considerable photostability and chemical stability. The Cs_4PbBr_6 PNCs are obtained via direct ultrasonication of precursors or after adding OAm in the pre-synthesized $CsPbBr_3$ PNCs solution. The phase transformation of orthorhombic $CsPbBr_3$ NCs to rhombohedral Cs_4PbBr_6 NCs is promoted by the capacity of organic ligands to dissolve $PbBr_2$, and by the formation of lead oleate and the dissociation of $CsPbBr_3$ PNCs. Morphology changes are mainly ascribed to the anisotropic growth of the crystals. In addition, a reverse transformation from Cs_4PbBr_6 PNCs to $CsPbBr_3$ PNCs can be achieved by adding water to pre-synthesized Cs_4PbBr_6

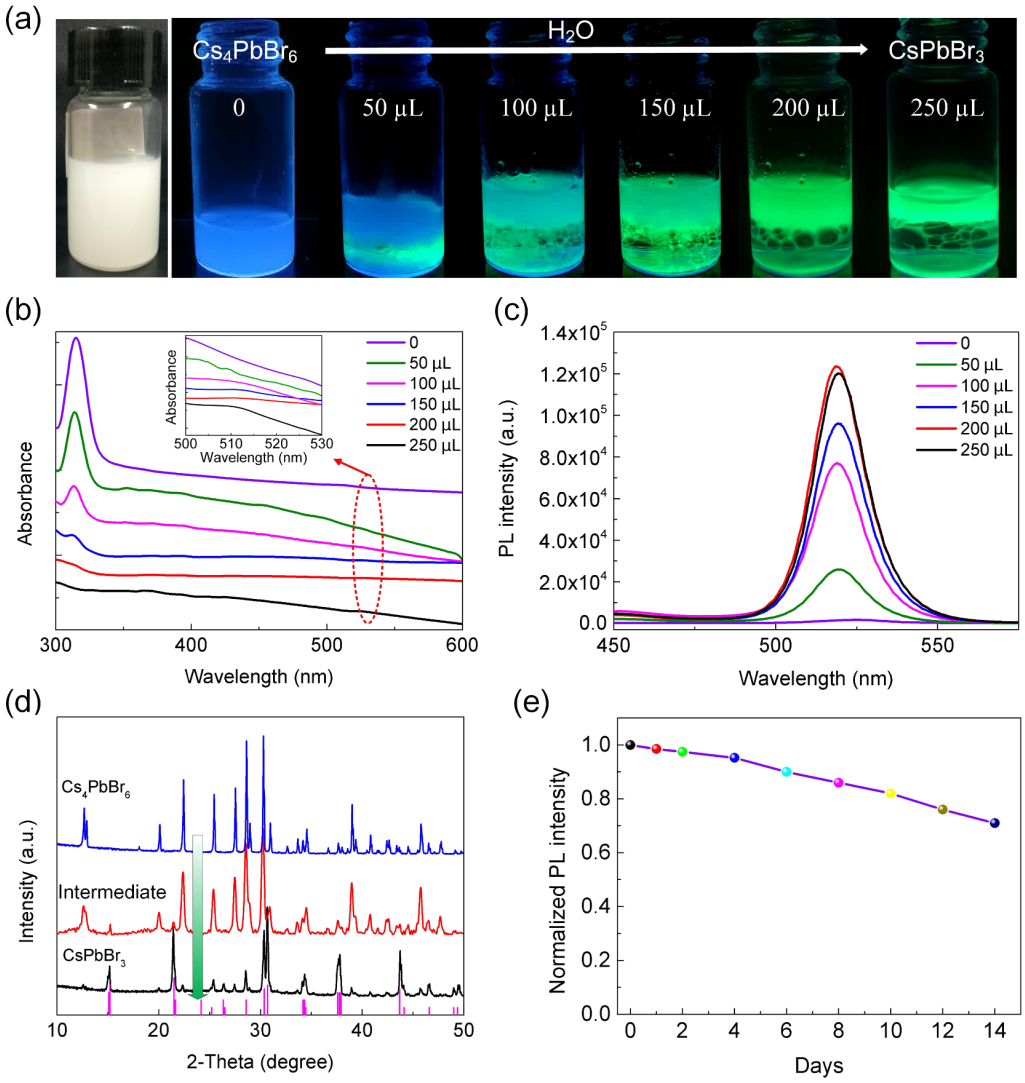

Figure 6: (a) The transformation process from Cs_4PbBr_6 PNCs to $CsPbBr_3$ PNCs. The products were illuminated under a 365 nm UV light. Both (b) UV–vis absorption spectra and (c) PL spectra of products were recorded during the transformation process. (d) XRD diffraction patterns of typical products prepared by changing the amount of added water, demonstrating the transformation from rhombohedral Cs_4PbBr_6 PNCs to orthorhombic $CsPbBr_3$ PNCs. (e) Stability of as-prepared $CsPbBr_3$ PNCs in ambient environment.

PNCs. The developed ultrasonication assistance results in the successful control over the phase transformation of PNCs, which can find widespread application in photoelectronic devices. We anticipate that this work can be extended to prepare other halide perovskites.

Experimental

Chemicals

Cesium carbonate (Cs_2CO_3, 99%), lead bromide ($PbBr_2$, 98%), liquid paraffin (90%), oleic acid (OA, 90%), oleylamine (OAm, 70%), and anhydrous toluene (99.8%) were purchased from Shanghai Aladdin Biochemical Technology Co. The chemicals used in the present work were of analytical grade and used without further purifications.

Synthesis of $CsPbBr_3$ PNCs and Cs_4PbBr_6 PNCs

$CsPbBr_3$ PNCs: The PNCs were prepared via modifying the procedures reported by Tong and Rao and co-workers [29,30]. In a typical process, Cs_2CO_3 (0.15 mmol) and $PbBr_2$ (0.30 mmol) powders were added to a mixture of 10 mL liquid paraffin (LP), 0.50 mL OA and 0.50 mL OAm. Then the reaction medium was processed by tip-sonication at a power of 120 W for 40 min. During the sonication, the colorless reaction medium gradually transformed into a yellow and then an orange-yellow solution, which suggests the formation of PNCs and demonstrates strong fluorescence emission under 365 nm UV light excitation. After completion of the reaction, unreacted precursors and excess ligands were removed by centrifugation

at a speed of 3000 rpm for 10 min and then the precipitate was redispersed in 5.0 mL of toluene. Then, the colloidal solution was centrifuged at a speed of 12000 rpm for 5 min and the sediment was redispersed in toluene for further characterization.

Cs_4PbBr_6 PNCs: Cs_2CO_3 (0.15 mmol) and $PbBr_2$ (0.30 mmol) powders were added to a mixture of 10 mL liquid paraffin, 0.50 mL OA and 3.0 mL OAm, while keeping other synthesis conditions as the same as that of $CsPbBr_3$ PNCs.

Reversible transformation from Cs_4PbBr_6 PNCs to $CsPbBr_3$ PNCs

50–250 μL of water was added to 5.0 mL of the pre-synthesized Cs_4PbBr_6 PNCs solution and shaken slightly, which is a modification of the work reported by Wu and co-workers [20].

Characterizations

The crystal surface morphology of the PNCs was characterized by transmission electron microscopy (TEM, JEM-2100F, JEOL, Japan) with an accelerating voltage of 100 kV. High-resolution TEM (HRTEM) was carried out on a JEOL JEM-2100F instrument operating at 200 kV. The crystal phases of the products were measured using an X-ray diffractometer (XRD, D8-Advance, Bruker, Germany) with a Cu Kα radiation source (λ = 0.15418 nm) at a counting rate of 2° per minute in the scanning angle (2θ) range from 5° to 50°. The surface morphology of Cs_4PbBr_6 PNCs was characterized by using a field-emission scanning electron microscope (SEM, Merlin). The UV–vis absorption spectra of the samples were measured using a UV–vis spectrometer (Shimadzu, Japan) over the wavelength range from 300 to 700 nm, at 1 nm intervals. The PL spectra of the PNCs were recorded using a fluorescence spectrophotometer (RF-6000, Shimadzu, Japan) using a Xe lamp as an excitation source.

Supporting Information

Supporting Information File 1

Additional PL spectra, SEM image, and UV–vis absorption spectra.
[https://www.beilstein-journals.org/bjnano/content/supplementary/2190-4286-10-66-S1.pdf]

Supporting Information File 2

Video showing the transformation from Cs_4PbBr_6 to $CsPbBr_3$ PNCs after addition of water.
[https://www.beilstein-journals.org/bjnano/content/supplementary/2190-4286-10-66-S2.mp4]

Acknowledgements

This work is financially supported by National Natural Science Foundation of China (51735004, 51805173, and 51775199), Natural Science Foundation of Guangdong Province (2014A030312017), Science & Technology Program of Guangdong Province (2017B010115001), and the SCUT Fundamental Research Funds for the Central Universities.

ORCID® iDs

Jin Z. Zhang - https://orcid.org/0000-0003-3437-912X

References

1. Pan, J.; Quan, L. N.; Zhao, Y.; Peng, W.; Murali, B.; Sarmah, S. P.; Yuan, M.; Sinatra, L.; Alyami, N. M.; Liu, J.; Yassitepe, E.; Yang, Z.; Voznyy, O.; Comin, R.; Hedhili, M. N.; Mohammed, O. F.; Lu, Z. H.; Kim, D. H.; Sargent, E. H.; Bakr, O. M. *Adv. Mater. (Weinheim, Ger.)* **2016,** *28,* 8718–8725. doi:10.1002/adma.201600784
2. Li, J.; Xu, L.; Wang, T.; Song, J.; Chen, J.; Xue, J.; Dong, Y.; Cai, B.; Shan, Q.; Han, B.; Zeng, H. *Adv. Mater. (Weinheim, Ger.)* **2017,** *29,* 1603885. doi:10.1002/adma.201603885
3. Jeon, N. J.; Na, H.; Jung, E. H.; Yang, T.-Y.; Lee, Y. G.; Kim, G.; Shin, H.-W.; Il Seok, S.; Lee, J.; Seo, J. *Nat. Energy* **2018,** *3,* 682–689. doi:10.1038/s41560-018-0200-6
4. Wang, X.; Shoaib, M.; Wang, X.; Zhang, X.; He, M.; Luo, Z.; Zheng, W.; Li, H.; Yang, T.; Zhu, X.; Ma, L.; Pan, A. *ACS Nano* **2018,** *12,* 6170–6178. doi:10.1021/acsnano.8b02793
5. Yang, T.; Zheng, Y.; Du, Z.; Liu, W.; Yang, Z.; Gao, F.; Wang, L.; Chou, K.-C.; Hou, X.; Yang, W. *ACS Nano* **2018,** *12,* 1611–1617. doi:10.1021/acsnano.7b08201
6. Vickers, E. T.; Graham, T. A.; Chowdhury, A. H.; Bahrami, B.; Dreskin, B. W.; Lindley, S.; Bonabi Naghadeh, S.; Qiao, Q.; Zhang, J. Z. *ACS Energy Lett.* **2018,** *3,* 2931–2939. doi:10.1021/acsenergylett.8b01754
7. Koscher, B. A.; Swabeck, J. K.; Bronstein, N. D.; Alivisatos, A. P. *J. Am. Chem. Soc.* **2017,** *139,* 6566–6569. doi:10.1021/jacs.7b02817
8. Wu, K.; Liang, G.; Shang, Q.; Ren, Y.; Kong, D.; Lian, T. *J. Am. Chem. Soc.* **2015,** *137,* 12792–12795. doi:10.1021/jacs.5b08520
9. Akkerman, Q. A.; Park, S.; Radicchi, E.; Nunzi, F.; Mosconi, E.; De Angelis, F.; Brescia, R.; Rastogi, P.; Prato, M.; Manna, L. *Nano Lett.* **2017,** *17,* 1924–1930. doi:10.1021/acs.nanolett.6b05262
10. Yin, J.; Zhang, Y.; Bruno, A.; Soci, C.; Bakr, O. M.; Brédas, J.-L.; Mohammed, O. F. *ACS Energy Lett.* **2017,** *2,* 2805–2811. doi:10.1021/acsenergylett.7b01026
11. Yin, J.; Maity, P.; De Bastiani, M.; Dursun, I.; Bakr, O. M.; Brédas, J.-L.; Mohammed, O. F. *Sci. Adv.* **2017,** *3,* e1701793. doi:10.1126/sciadv.1701793
12. Saidaminov, M. I.; Almutlaq, J.; Sarmah, S.; Dursun, I.; Zhumekenov, A. A.; Begum, R.; Pan, J.; Cho, N.; Mohammed, O. F.; Bakr, O. M. *ACS Energy Lett.* **2016,** *1,* 840–845. doi:10.1021/acsenergylett.6b00396
13. Seth, S.; Samanta, A. *J. Phys. Chem. Lett.* **2017,** *8,* 4461–4467. doi:10.1021/acs.jpclett.7b02100
14. Protesescu, L.; Yakunin, S.; Bodnarchuk, M. I.; Krieg, F.; Caputo, R.; Hendon, C. H.; Yang, R. X.; Walsh, A.; Kovalenko, M. V. *Nano Lett.* **2015,** *15,* 3692–3696. doi:10.1021/nl5048779
15. Pan, A.; He, B.; Fan, X.; Liu, Z.; Urban, J. J.; Alivisatos, A. P.; He, L.; Liu, Y. *ACS Nano* **2016,** *10,* 7943–7954. doi:10.1021/acsnano.6b03863

16. He, X.; Qiu, Y.; Yang, S. *Adv. Mater. (Weinheim, Ger.)* **2017,** *29,* 1700775. doi:10.1002/adma.201700775
17. Bekenstein, Y.; Koscher, B. A.; Eaton, S. W.; Yang, P.; Alivisatos, A. P. *J. Am. Chem. Soc.* **2015,** *137,* 16008–16011. doi:10.1021/jacs.5b11199
18. Chen, M.; Zou, Y.; Wu, L.; Pan, Q.; Yang, D.; Hu, H.; Tan, Y.; Zhong, Q.; Xu, Y.; Liu, H.; Sun, B.; Zhang, Q. *Adv. Funct. Mater.* **2017,** *27,* 1701121. doi:10.1002/adfm.201701121
19. Rao, L.; Tang, Y.; Yan, C.; Li, J.; Zhong, G.; Tang, K.; Yu, B.; Li, Z.; Zhang, J. Z. *J. Mater. Chem. C* **2018,** *6,* 5375–5383. doi:10.1039/c8tc00582f
20. Wu, L.; Hu, H.; Xu, Y.; Jiang, S.; Chen, M.; Zhong, Q.; Yang, D.; Liu, Q.; Zhao, Y.; Sun, B.; Zhang, Q.; Yin, Y. *Nano Lett.* **2017,** *17,* 5799–5804. doi:10.1021/acs.nanolett.7b02896
21. Palazon, F.; Urso, C.; De Trizio, L.; Akkerman, Q.; Marras, S.; Locardi, F.; Nelli, I.; Ferretti, M.; Prato, M.; Manna, L. *ACS Energy Lett.* **2017,** *2,* 2445–2448. doi:10.1021/acsenergylett.7b00842
22. Palazon, F.; Almeida, G.; Akkerman, Q. A.; De Trizio, L.; Dang, Z.; Prato, M.; Manna, L. *Chem. Mater.* **2017,** *29,* 4167–4171. doi:10.1021/acs.chemmater.7b00895
23. Zhai, W.; Lin, J.; Li, Q.; Zheng, K.; Huang, Y.; Yao, Y.; He, X.; Li, L.; Yu, C.; Liu, C.; Fang, Y.; Liu, Z.; Tang, C. *Chem. Mater.* **2018,** *30,* 3714–3721. doi:10.1021/acs.chemmater.8b00612
24. Liu, Z.; Bekenstein, Y.; Ye, X.; Nguyen, S. C.; Swabeck, J.; Zhang, D.; Lee, S.-T.; Yang, P.; Ma, W.; Alivisatos, A. P. *J. Am. Chem. Soc.* **2017,** *139,* 5309–5312. doi:10.1021/jacs.7b01409
25. Udayabhaskararao, T.; Houben, L.; Cohen, H.; Menahem, M.; Pinkas, I.; Avram, L.; Wolf, T.; Teitelboim, A.; Leskes, M.; Yaffe, O.; Oron, D.; Kazes, M. *Chem. Mater.* **2018,** *30,* 84–93. doi:10.1021/acs.chemmater.7b02425
26. Huang, H.; Xue, Q.; Chen, B.; Xiong, Y.; Schneider, J.; Zhi, C.; Zhong, H.; Rogach, A. L. *Angew. Chem.* **2017,** *129,* 9699–9704. doi:10.1002/ange.201705595
27. Fang, F.; Chen, W.; Li, Y.; Liu, H.; Mei, M.; Zhang, R.; Hao, J.; Mikita, M.; Cao, W.; Pan, R.; Wang, K.; Sun, X. W. *Adv. Funct. Mater.* **2018,** *28,* 1706000. doi:10.1002/adfm.201706000
28. Li, X.; Yu, D.; Cao, F.; Gu, Y.; Wei, Y.; Wu, Y.; Song, J.; Zeng, H. *Adv. Funct. Mater.* **2016,** *26,* 5903–5912. doi:10.1002/adfm.201601571
29. Tong, Y.; Bladt, E.; Aygüler, M. F.; Manzi, A.; Milowska, K. Z.; Hintermayr, V. A.; Docampo, P.; Bals, S.; Urban, A. S.; Polavarapu, L.; Feldmann, J. *Angew. Chem., Int. Ed.* **2016,** *55,* 13887–13892. doi:10.1002/anie.201605909
30. Rao, L.; Tang, Y.; Song, C.; Xu, K.; Vickers, E. T.; Bonabi Naghadeh, S.; Ding, X.; Li, Z.; Zhang, J. Z. *Chem. Mater.* **2019,** *31,* 365–375. doi:10.1021/acs.chemmater.8b03298
31. Brouwer, A. M. *Pure Appl. Chem.* **2011,** *83,* 2213–2228. doi:10.1351/pac-rep-10-09-31
32. Qi, X.; Zhou, T.; Deng, S.; Zong, G.; Yao, X.; Fu, Q. *J. Mater. Sci.* **2014,** *49,* 1785–1793. doi:10.1007/s10853-013-7866-8
33. Mphuthi, N. G.; Adekunle, A. S.; Fayemi, O. E.; Olasunkanmi, L. O.; Ebenso, E. E. *Sci. Rep.* **2017,** *7,* 43181. doi:10.1038/srep43181
34. Yuwen, L.; Yu, H.; Yang, X.; Zhou, J.; Zhang, Q.; Zhang, Y.; Luo, Z.; Su, S.; Wang, L. *Chem. Commun.* **2016,** *52,* 529–532. doi:10.1039/c5cc07301d
35. Akkerman, Q. A.; Motti, S. G.; Srimath Kandada, A. R.; Mosconi, E.; D'Innocenzo, V.; Bertoni, G.; Marras, S.; Kamino, B. A.; Miranda, L.; De Angelis, F.; Petrozza, A.; Prato, M.; Manna, L. *J. Am. Chem. Soc.* **2016,** *138,* 1010–1016. doi:10.1021/jacs.5b12124
36. Dang, Z.; Shamsi, J.; Palazon, F.; Imran, M.; Akkerman, Q. A.; Park, S.; Bertoni, G.; Prato, M.; Brescia, R.; Manna, L. *ACS Nano* **2017,** *11,* 2124–2132. doi:10.1021/acsnano.6b08324
37. Seth, S.; Samanta, A. *J. Phys. Chem. Lett.* **2018,** *9,* 176–183. doi:10.1021/acs.jpclett.7b02931
38. Akkerman, Q. A.; Abdelhady, A. L.; Manna, L. *J. Phys. Chem. Lett.* **2018,** *9,* 2326–2337. doi:10.1021/acs.jpclett.8b00572
39. Zhang, Y.; Saidaminov, M. I.; Dursun, I.; Yang, H.; Murali, B.; Alarousu, E.; Yengel, E.; Alshankiti, B. A.; Bakr, O. M.; Mohammed, O. F. *J. Phys. Chem. Lett.* **2017,** *8,* 961–965. doi:10.1021/acs.jpclett.7b00105
40. Chen, D.; Wan, Z.; Chen, X.; Yuan, Y.; Zhong, J. *J. Mater. Chem. C* **2016,** *4,* 10646–10653. doi:10.1039/c6tc04036e
41. Almeida, G.; Goldoni, L.; Akkerman, Q.; Dang, Z.; Khan, A. H.; Marras, S.; Moreels, I.; Manna, L. *ACS Nano* **2018,** *12,* 1704–1711. doi:10.1021/acsnano.7b08357
42. Koolyk, M.; Amgar, D.; Aharon, S.; Etgar, L. *Nanoscale* **2016,** *8,* 6403–6409. doi:10.1039/c5nr09127f
43. Liang, Z.; Zhao, S.; Xu, Z.; Qiao, B.; Song, P.; Gao, D.; Xu, X. *ACS Appl. Mater. Interfaces* **2016,** *8,* 28824–28830. doi:10.1021/acsami.6b08528
44. Liu, W.; Zheng, J.; Cao, S.; Wang, L.; Gao, F.; Chou, K.-C.; Hou, X.; Yang, W. *Inorg. Chem.* **2018,** *57,* 1598–1603. doi:10.1021/acs.inorgchem.7b02941
45. Li, G.; Wang, H.; Zhu, Z.; Chang, Y.; Zhang, T.; Song, Z.; Jiang, Y. *Chem. Commun.* **2016,** *52,* 11296–11299. doi:10.1039/c6cc05877a

License and Terms